POLITECNICO
MILANO 1863

Post-Print

This is the accepted version of:

When citing this work, cite the original published paper.

Non-linear Aeroelastic Capabilities in NeoCASS Suite

Francesco Toffol[1] and Sergio Ricci[2]
Politecnico di Milano, Department of Aerospace Science and Technology, via la Masa 34, 20156, Milano, Italy.

Highly flexible wing may experience large deflection such that the linear analysis methods are not valid anymore. The results obtained with classical aeroelastic solution are strongly affected by the large deflection experienced during flight and they may provide wrong results, jeopardizing the aircraft. Large deflection affects the static solution e.g. trim, but the pre-stress effect impacts on the modal base used to evaluate the dynamic response and flutter behavior.

I. Introduction

The fight against the climate changes asks to the aeronautical industry to cut its portion of pollutant emissions. To do that, more efficient aircraft must be designed, fully exploiting new materials and technologies, and investigating breakthrough configurations. From the configuration perspective, many solutions were proposed in the recent years like the Blended Wing Body[1][2][3] the Truss-Braced Wing [4]-[7], the Box Wing [9][10], and many others. In many cases, the designers proposed to increase significantly the aspect ratio to minimize the induced drag component for an improved efficiency of the aircraft [11]-[14]. This is possible thanks to the exploitation of composite material [15] and the production process used e.g. fiber placing. These new aircraft configurations have slender and highly flexible wings that experience large deflection when loaded with aerodynamic and inertial loads, reaching wing tip deflection >10% of the wingspan, commonly considered as the validity limit of linear analysis.

In case of highly flexible structures, a non-linear approach should be used to account for the aeroelastic effects due to large deformations. From a structural design point of view, the deformability of the aircraft should be considered since the beginning of the aircraft design process, where the usage of traditional coupled Non-Linear FEM and CFD solvers would be extremely time consuming. For this reason, in the last years many efforts were concentrated in the developing of medium fidelity non-linear aeroelastic solvers: University of Michigan developed an in-house non-linear aeroelastic solver [16]-[18], Imperial College implemented another one called SHARPy [19], also DLR worked on this topic [20][21], and Technion with the Modal Rotation Method (MRM) [22][23].

The new analysis capabilities must be integrated with the conceptual design suites, to include non-linear aeroelastic investigation and verification into the design loop. Different tools for conceptual and design are available and are described in literature, such as: TU-Delft PROTEUS [24], Bombardier in-house tool [25], Gulfstream ATLASS [26], EMWET [27], and many others. By now, a tool that combines in an easy and fast way non-linear analysis capabilities is still missing. NeoCASS [28]-[31] is the physical based design tool developed by the Politecnico of Milano, which underwent major revision [32] in the last years and additional features have been added [33]-[36]. In NeoCASS there are implemented the majority of the linear aeroelastic solver (trim, dynamic response, flutter, etc.), but a non-linear aeroelastic solver was not available until today. To fill this gap , a brand-new non-linear solver was developed and implemented, bridging the gap between the non-linear analysis tools and the conceptual design suites. The result is a single environment- single model analysis tool that can perform sizing and analysis concurrently.

II. Methodology and Validation

This section describes the methodology used to develop the non-linear analysis suite encompassed in NeoCASS. It is divided in three main sub-sections, where each analysis step is explained and validated.

The tool is part of the NeoCASS suite, where a three nodes non-linear beam finite volume is implemented for the structural FEM model [37]. To preserve the continuity of the topic treated, the next sections present the methodology adopted for each solver and its validation in the same section, so four of them are present: Non-Linear Static Solver,

---

[1] Post-Doctoral research fellow, Politecnico di Milano, Department of Aerospace Science and Technology, via la Masa 34, 20156, Milano, Italy

[2] Full Professor, Department of Aerospace Science and Technology, Politecnico di Milano, Department of Aerospace Science and Technology, via la Masa 34, 20156, Milano, Italy. AIAA Senior Member

Modal Solver, Aero-elastic Non-Linear solver and finally the Flutter solver for the prestressed structure. An additional section is added to describe the Fluid-Structure Interface (FSI).

The test case chosen to validate the solvers is the Pre-Pazy wing [38] developed in the framework of NASA's Aeroleastic Prediction Workshop 3 (AePW-3), Large Deflection Working Group (LDWG) [39].

A. Non-Linear Static Solver

The static solver developed and implemented reply to the need of having a tool able to manage large deflection with small strains and linear constitutive law. It is based on the non-linear finite volume beam presented in [37], which is currently implemented in NeoCASS in its linear version.
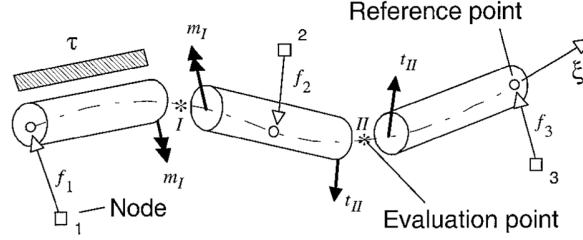

Figure 1: Finite volume three-node beam from [37]

Recalling the approach adopted in [37], the equilibrium for the finite volume beam is represented by Eq. (1), where A is an arm matrix between the nodes and the collocation points, D is an arbitrary beam linear constitutive matrix 6x6, Ψ the vector containing the generalized strains and curvatures and F_{ext} the vector of the external applied loads.

$$AD\Psi = F_{ext} \qquad (1)$$

The internal forces on the evaluation points are obtained through the constitutive law as $\theta = D\Psi$, hence Eq.(1) that comes from a weak formulation of the beam element equilibrium, that simply states that the internal forces at the evaluation points equilibrates the external loads applied on the nodes.

In linear case, the generalized strains can be related to the nodal displacements and rotations x, leading to the well-known force/displacement relation in Eq.(2)

$$AD\Xi x = F_{ext} \Rightarrow Kx = F_{ext} \qquad (2)$$

Since the linear approximation is not valid in case of large displacement, a linearization of the problem, e.g. through Taylor's series expansion is needed. Following the more familiar FEM matrix notation of Eq.(2), the problem can be reduced to its linearized form of Eq.(3), where K_L is the linear strain incremental stiffness matrix and K_{NL} is the non-linear strain (geometric or initial stress) incremental stiffness matrix. The F_{nodal} collects the nodal forces equivalent to the stresses.

$$(K_L + K_{NL})x = F_{ext} - F_{nodal} \Rightarrow K_t x = r \qquad (3)$$

Since an Updated Lagrangian (UL) approach is used, all the terms are computed on the deformed configuration and x represents the incremental displacement w.r.t. the deformed equilibrium configuration.

The linear problem in Eq.(3) is solve iteratively until the equilibrium is satisfied i.e., the external forces are in equilibrium with the internal ones and the right-hand side of Eq.(3) goes to zero, i.e. the residual r is null.

To improve the convergency of the solution the load is applied with a user defined load sequence, for example ten equally distributed load step (10% load increment). The equilibrium is satisfied for each load step, and at the end of each step the new reference condition is obtained following the UL approach. This is iterated until the load sequence is completed.

Despite the beam's formulation manages large rotations, the constraints mechanism for the rigid elements (like the Nastran's RBE2) may introduce significant error in the displacement of slave DOFs. The displacement of the slave node is the sum of the master's displacement and the cross product between the connecting arm and the master rotation, as in Eq. (4).

$$x_{slave} = x_{master} + \phi_{master} \times (p_{slave} - p_{master}) \qquad (4)$$

As an example, Figure 2 shows the error that the linearization of the rotation introduces: simulating an UL approach with different incremental rotation Figure 2 (a) shows the error on the final position for a cumulative rotation of 360° with unit radius. The final error is sensitive to the rotation increment, and for whichever increment the behaviour is

2

divergent, as the spiral in Figure 2(c) shows. It must be pointed out that for small rotation (<15°) and with small rotation increment, the linearized approximation is still valid, as the zoom in Figure 2 (b) shows, hence the rigid connections can be used but particular attention has to be paid, especially in the load step discretization and in the rotation achieved.
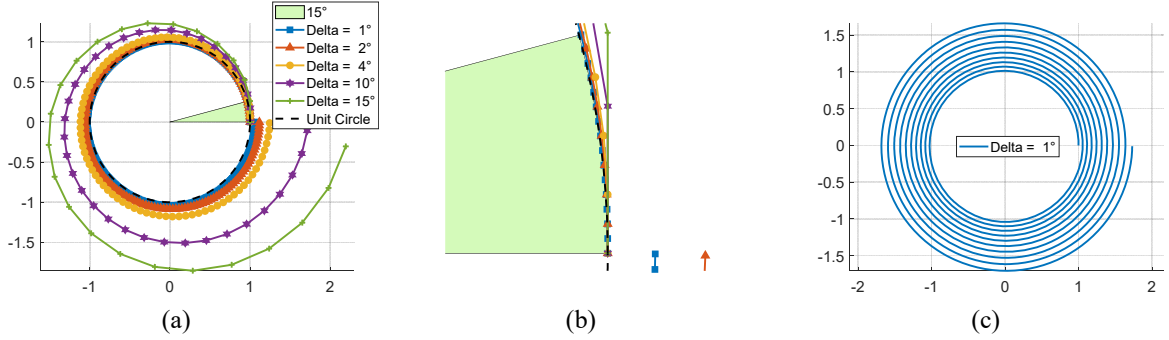

(a)

(b)

(c)

Figure 2: Linearized rotation approximation error: (a) single revolution, different rotation increments; (b) zoom in the 15° region; (c) diverging behavior on 10 revolutions with 1° increment

During the solution process, the linear constraint matrix T_{gz} is updated for each iteration and it is used to reduce the global degree of freedom matrices, indicated with the *gg* subscripts, into the analysis set indicated by *zz* subscripts.

$$K_{zz} = T_{gz}^T K_{gg} T_{gz} \qquad (5)$$

Despite the linear(ized) constraints matrix may introduce errors in the solution, it is still convenient its implementation to keep a linear formulation for the constraints.

The solver implemented is validated using as test case the numerical and experimental results obtained in [40].

The Pre-Pazy Wing FEM model in Figure 3, based on the geometrical, stiffness and mass properties described in [41], is loaded on its tip with a concentrated force equivalent to the mass hung in the experiment. Two chordwise loading point were used: the first one is coincident with the elastic axis to reproduce a pure bending test, while the second one is moved forward to introduce a torque, that is combined with the bending.
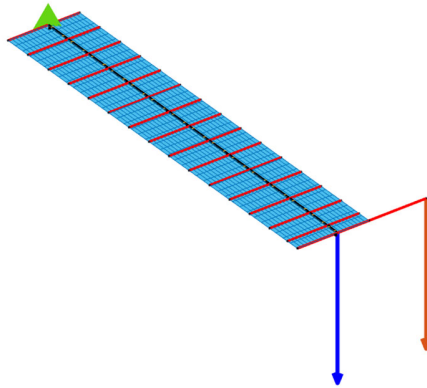

Figure 3: Pre-Pazy Wing tip loading for bending (blue arrow) and torsion (red arrow)

The comparison between the results obtained with NeoCASS and other non-linear solvers, like UM/NAST , SHARPy, and MRM; as well as the experimental measurement provided by Technion, are illustrated in Figure 4: (a) shows the tip vertical displacement for the bending test, while the results for the bending-torsion test are presented in (b) as vertical displacement and in (c) as tip rotation around beam's axis: The displacement is normalized w.r.t. the wing span of 0.55m, showing a maximum displacement that is half of the wing span. The displacement differences for zero loading are because UM/NAST, SHARPy and NeoCASS account for the gravity, while the gravity effect is not accounted in MRM, and it is not measured experimentally. The results obtained with NeoCASS are identical to the one obtained with UM/NAST and SHARPy, validating the implementation of the non-linear static solver here presented.
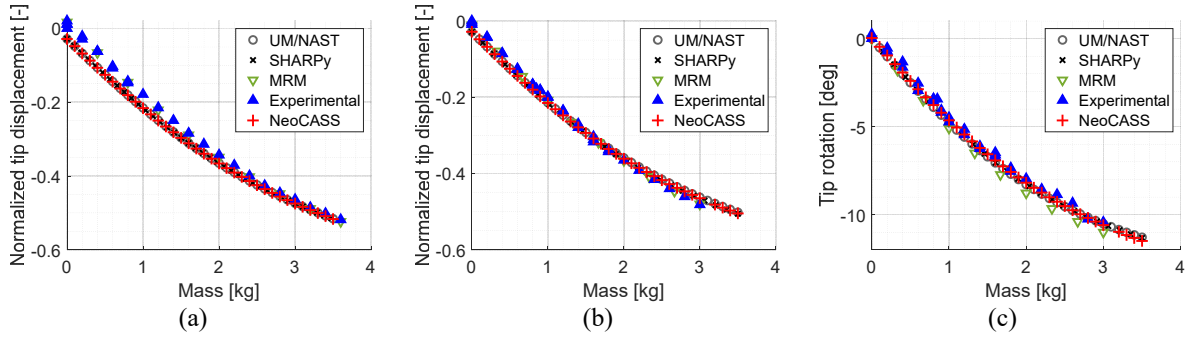
3

Figure 4: Non-linear solution for tip loading: (a) pure bending test tip vertical displacement (b) bending-torsion test tip vertical displacement (c) bending-torsion test tip rotation

In addition to the displacements, the non-linear solver provides the tangential stiffness K_t matrix i.e., the stiffness matrix in the deformed configuration that accounts for the K_{NL} term, that is the non-linear strain (geometric or initial stress) incremental stiffness matrix. This non-linear stiffness term becomes relevant when dynamic simulations on highly flexible structures are performed, as explained in the next sections.

B. Modal analysis of prestressed structure

The modal solver implement in NeoCASS is not modified and it is based on the classical eigenvalue solution of an elastic system with the only stiffness and mass terms. The model used to perform the analysis is modified to account for the K_{NL} term, and to consider the mass matrix computed in the deformed configuration. The eigenvalue problem becomes the one in Eq.(6)

$$K_t X = \Lambda M_{defo} X \Rightarrow \left(K_t - \Lambda M_{defo} \right) X = 0 \tag{6}$$

In this way the modal analysis becomes solution dependent, meaning that the dynamic properties in term of eigenvalues and eigenvectors depend on the static equilibrium achieved by the non-linear static solution.

As a validation example, the dynamic properties of the Pre-Pazy wing for different tip loads, as in Figure 3, are computed. The results, presented in Figure 5, are compared with the one obtained with SHARPy, UM/NAST and MRM: The frequencies of the first 5 modes (4 for MRM) are well matched across the whole load envelope (0-30N).
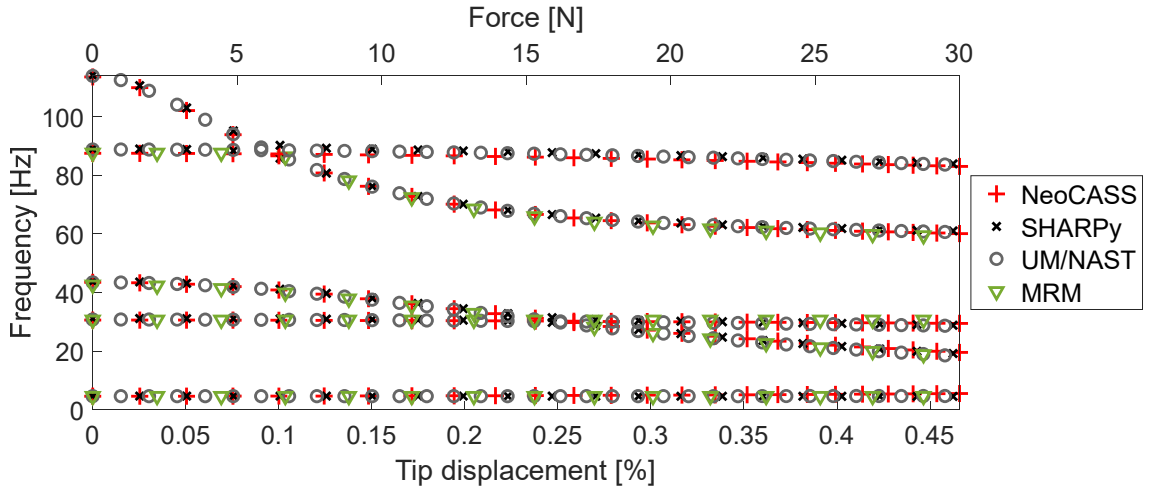

Figure 5: Modal frequencies evolution with increasing tip load

The pre-stress effect introduced is noticeable and affects the evolution of the eigenvalues with the load. Moreover, it affects the eigenvectors or modal shapes, as in Figure 6: the (a-c) figures are the first three modes obtained for the unloaded structure, while (d-f) show the first three modes for the structure loaded with 30N. It is possible to see how the prestress affects the modal shapes as well: the pure torsion mode of (c) couples with the in-plane bending as in (e) and appears in a different position (2nd instead of 3rd). The difference between the modal based is remarked by Figure

4

7 where the Modal Assurance Criterion (MAC as in Eq.(7)) matrices are presented: (a) shows the auto-MAC matrix for the unloaded structure, while (b) is the cross-MAC matrix between the unloaded structure (Linear) and the structure loaded with 30N (Non-Linear). As graphically noted in Figure 6, the coupling between the torsion and in-plane mode is relevant, and the other cross-MAC matrix term shows that the prestressed modal base changes with respect to the unloaded one.

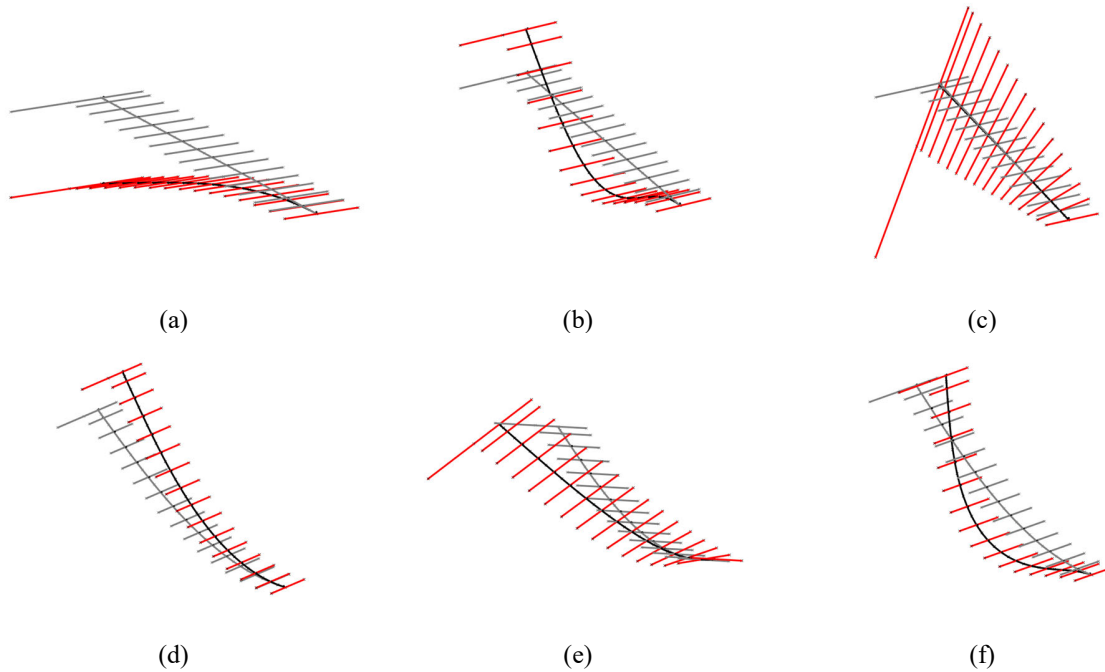$$MAC(i,j) = \frac{|\Phi_i \Phi_j|^2}{(\Phi_i \Phi_i)(\Phi_j \Phi_j)} \qquad (7)$$

| (a) | (b) | (c) |

| (d) | (e) | (f) |

Figure 6: (a-c) first 3 modes for the unloaded structure, (d-f) first 3 modes for the structure loaded with 30N
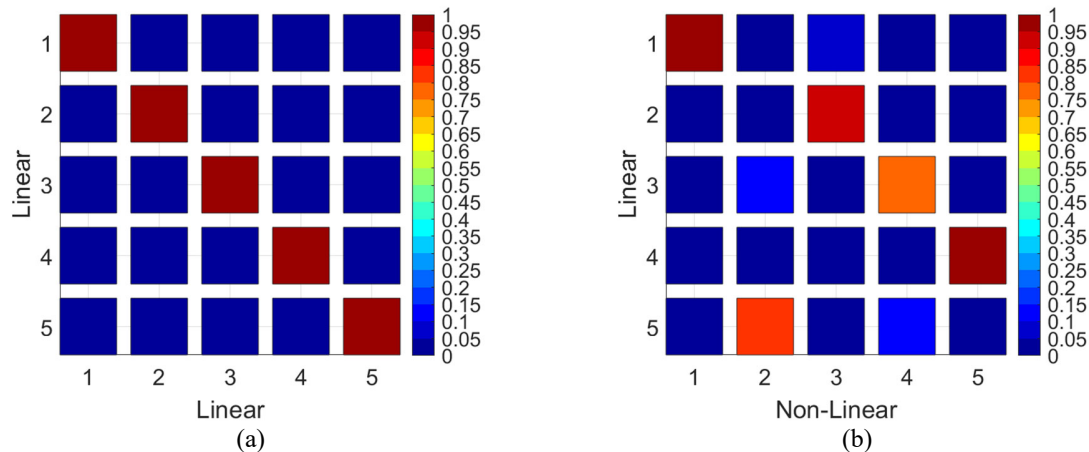

(a)

(b)

Figure 7: MAC matrices: (a) auto-MAC matrix for the unloaded structure (b) cross-MAC matrix between unloaded structure (Linear) and structure loaded with 30N (Non-Linear)

This validation step shows how the prestress and deformed mass matrices are computed and exported to perform modal analysis on a deformed structure. In this way it is possible to obtain a modal based of an equilibrium configuration and perform linear dynamic analysis around it, by using the prestressed modal base to reduce the model

order. This capability is fundamental to perform flutter analysis on deformed configuration and is one of the solution steps required for such application, the other brick is the non-linear aeroelastic solver presented in the next section.

C. Fluid Structure Interface

The aerodynamics methods implemented in NeoCASS, that are Vortex and Doublet Lattice Method (VLM & DLM), have a mesh which is topologically different w.r.t. the structural one. The connection between the structural and aerodynamic worlds is provided by the splines, which are based on the Radial Basis Function [42] approach to transfer the displacement and the loads between the two disciplines.

In general, splining techniques provide a matrix that transforms structural displacements into deformation of the aerodynamic mesh as in Eq.(8), where the H_{as} is computed by the spline method adopted, RBF in our case. The H_{as} matrix is computed for each UL step, keeping the spline scheme updated and deforming the aerodynamic mesh consequently.

$$X_{aero} = H_{as}X_{structure} \qquad (8)$$

Figure 8 shows how the UL approach can deform the aerodynamic mesh following the structural displacements, both in the case of twist around the beam axis (a) and bending-like folding (b).
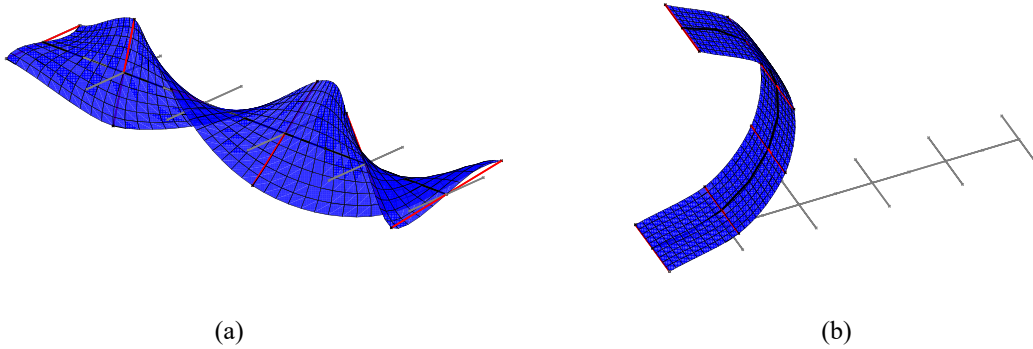

(a)   (b)

Figure 8: Aerodynamic mesh deformation under tip loading

D. Non-Linear Aero-Elastic Trim

The non-linear trim solution uses the same iterative scheme of the static solution, but in this case the external forces are function of the deformed configuration because the aerodynamic mesh and the structural model are updated at each load increment.

For each load step, a linear trim solution is performed and the loads acting on the structural nodes are computed. The loads are used as external load, solving a non-linear static problem as in section A. The main difference between the non-linear static solution is that after each load step solution, the external loads are re-computed performing a trim analysis on the result of the previous step deformed configuration. For example, the load used in the second load step are the one obtained on the deformed configuration on the first load step and then multiplied by the load scale factor n_j, used to compute the load fraction that must be used in the second step. In this way the loads are kept up to date, improving the convergency as illustrated in [17]. As described in section C, the FSI represented by the splines is updated at each load step, keeping the coherence between deformed structural and aerodynamic meshes.

The trim analysis can be performed in whichever constraint condition (free or constrained), in case of a trim analysis in free condition, the static non-linear solution must be performed substituting the reference point used for the mean axis computation [43] with an equivalent constraint.
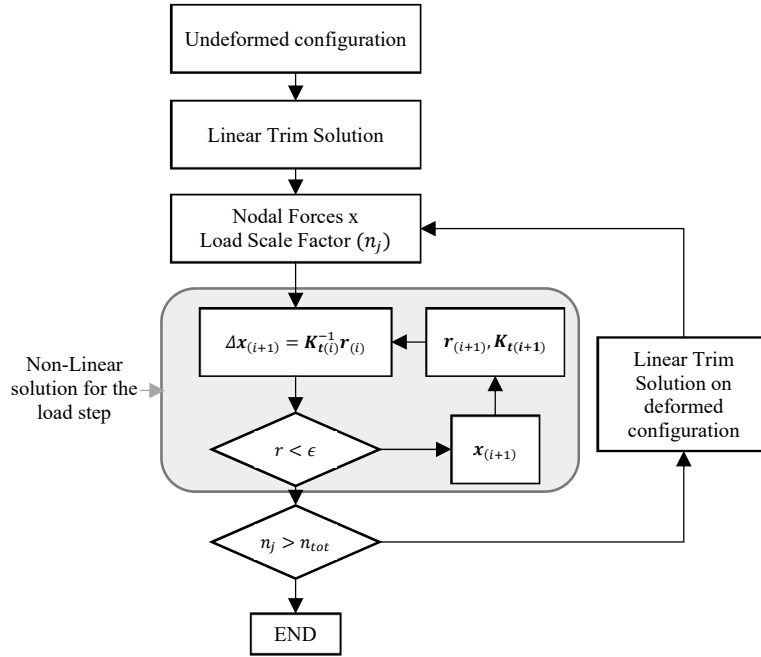The solution scheme is reported in Figure 9.

6

Figure 9: Non-linear trim solution scheme

Continuing the validation process, the non-linear trim solver was tested on the Pre-Pazy wing as done for the other steps. Two different attitudes were investigated, and the angle of attack considered are 5° and 7° respectively. The airspeed reaches $60\frac{m}{s}$ and the dynamic pressure is obtained considering a density of $\rho = 1.225\frac{kg}{m^3}$. Since the experiments were conduced with the wing vertically mounted, the gravity effect was neglected. For both the attitudes, the NeoCASS's results match the ones obtained with UM/NAST, SHARPy, MRM, and the experimental results measured by Technion, as illustrated in Figure 10.
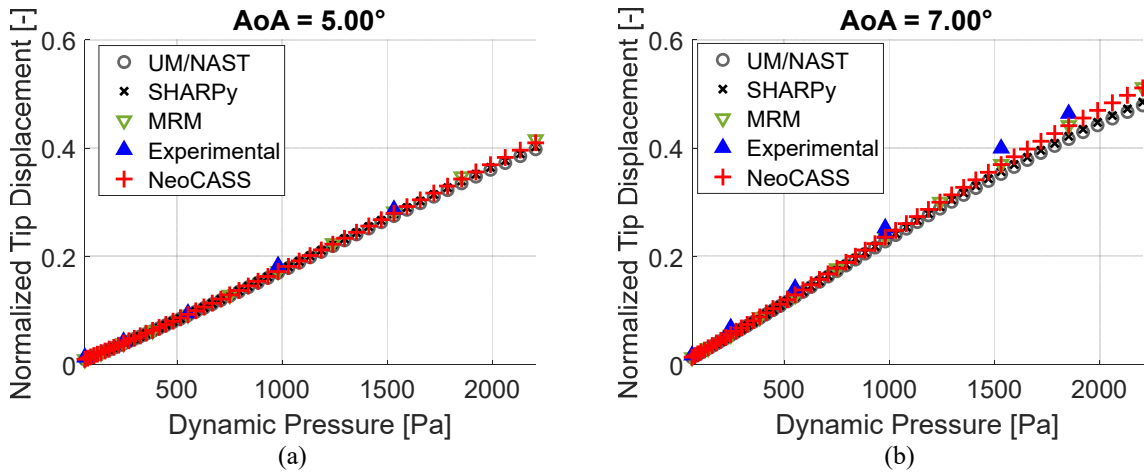

Figure 10 Pre-Pazy wing tip deflection compared with other solvers and experimental results: (a) AoA=5°; (b) AoA=7°

The non-linear solution over the whole airspeed range considered is presented in Figure 11 for both the attitudes considered (5° in (a) and 7° in (b)).

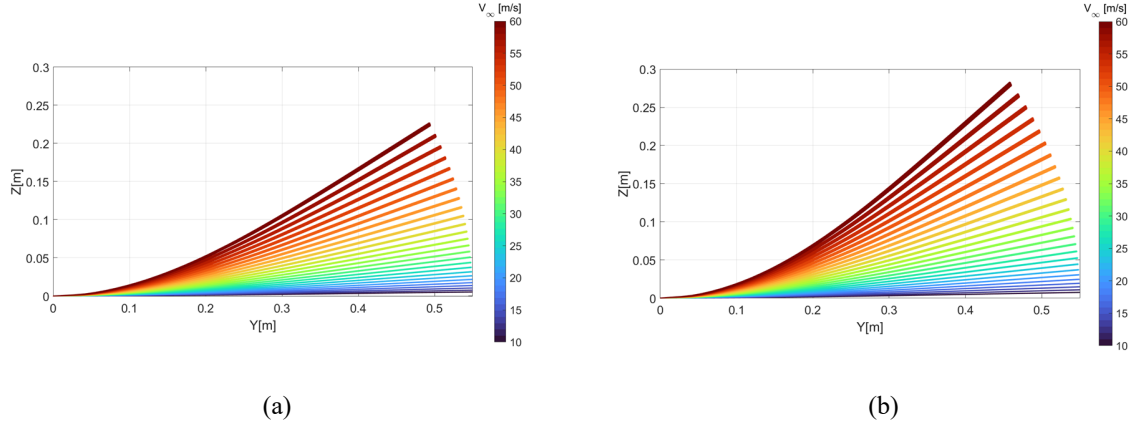*Figure 11: Deformed Pre-Pazy wing while increasing the airspeed: (a) AoA=5°; (b) AoA=7°*

As in the case of non-linear static solution, the tangential stiffness matrix K_t is an output and it can be used to compute the modal base of the equilibrium achieved with a non-linear trim solution. This latest aspect is fundamental to perform flutter computation on a deformed and prestressed structure.

E. Flutter analysis on prestressed and deformed configuration

In standard aeroelastic simulation codes, like Nastran, the flutter solution is performed solving the coupled FEM/DLM problem using dedicated numerical techniques. NeoCASS uses the DLM [44] for the unsteady generalized aerodynamic forces (GAFs), it accounts for the Mach dependency in the GAFs computation, but it needs a mesh which normals are orthogonal to the wind direction. For this reason, the DLM mesh deformed by the non-linear trim solution is modified to have the panels that are aligned with the wind direction. An example of this procedure is shown in Figure 12, where the DLM mesh deformed is re-aligned to the wind axis, in this case by neutralizing the twist effect. After the re-alignment of the mesh, the DLM solver provides the GAFs for the deformed configuration.
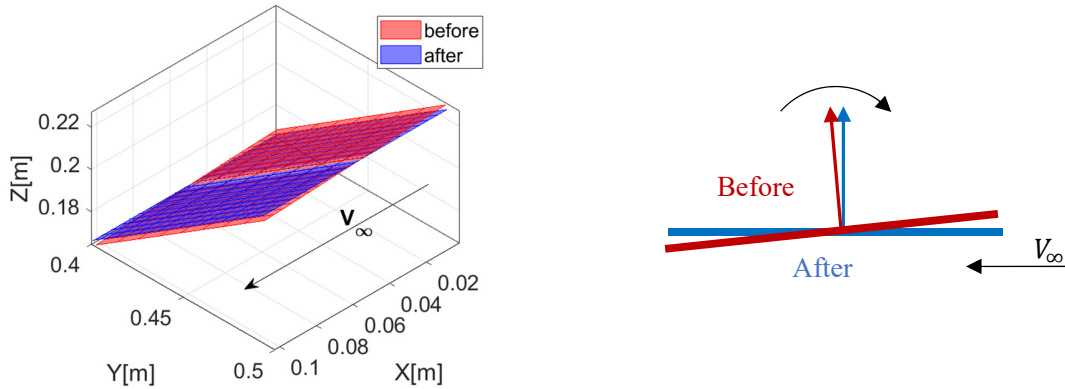

Figure 12: DLM mesh before (red) and after (blue) the alignment of the panel to the wind direction

Flutter analysis for prestressed configuration differs from the standard flutter solution because for each velocity step a different equilibrium configuration, provided by the non-linear trim solution, must be accounted to get the deformed structure and the prestressed modal base.

The algorithm used for the flutter solution is a conventional 2nd order p-k method, that solves the flutter equation for the single flight condition. In modal coordinates and in Laplace's coordinates the flutter problem becomes Eq.(9), where the modal matrices and aerodynamic matrices are computed for the deformed structure.

$$\left(ms^2 + cs + k - q_\infty H_{am}(p, M_\infty)\right)q(s) = 0 \Rightarrow F(s, V_\infty)q(s) = 0 \qquad (9)$$

The solution of the problem in Eq.(9) has *n* equation for *n+1* unknowns (*n* for *q* and 1 for *s*), for this reason a normalization equation for the eigenvectors in added to get a well posed non-linear (in *s*) problem, as Eq.(10).

$$\frac{1}{2}q^T q - 1 = 0 \qquad (10)$$

Eqs.(9)(10) provide the non-linear system which solution provides the map of the system's eigenvectors and eigenvalues for a given flight condition, determined by the non-linear trim solution.

The continuation method [45] originally implemented in NeoCASS loses its competitive advantage of following the single mode across the velocity envelope because the velocity is limited to a single point for each analysis.

The solution sequence, for each flight point is illustrated in Figure 13, while the result for each flight point is the solution to the flutter equation in terms of eigenvalues and eigenvectors λ_{fl}, X_{fl}.
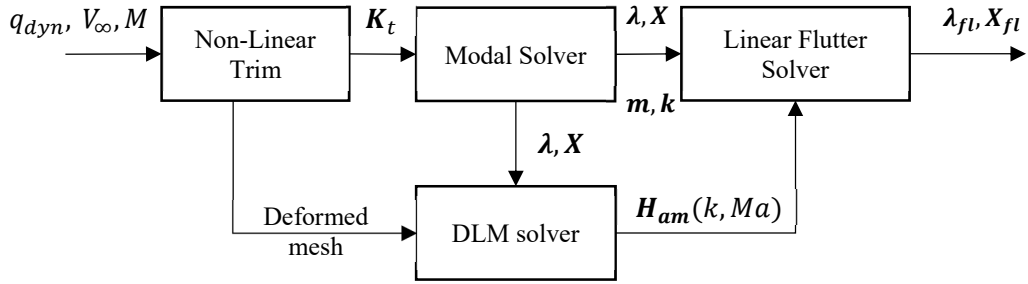

Figure 13: Scheme of the non-linear flutter solution

Following the philosophy adopted for the previous part of the paper, the flutter solver above presented was tested on the Pre-Pazy wing test case. The flight envelope reaches $V_\infty = 90\frac{m}{s}$ and covers the positive attitudes up to 5° of incidence. The flutter analysis performed on the undeformed solution provides a flutter speed $V_{f\ \alpha=0°} = 64.95\frac{m}{s}$. The results for the linear solution are illustrated in Figure 14. The solutions obtained with the two solvers, i.e. SHARpy and NeoCASSare similar both for the damping ratios and for the frequencies of the aeroelastic modes.
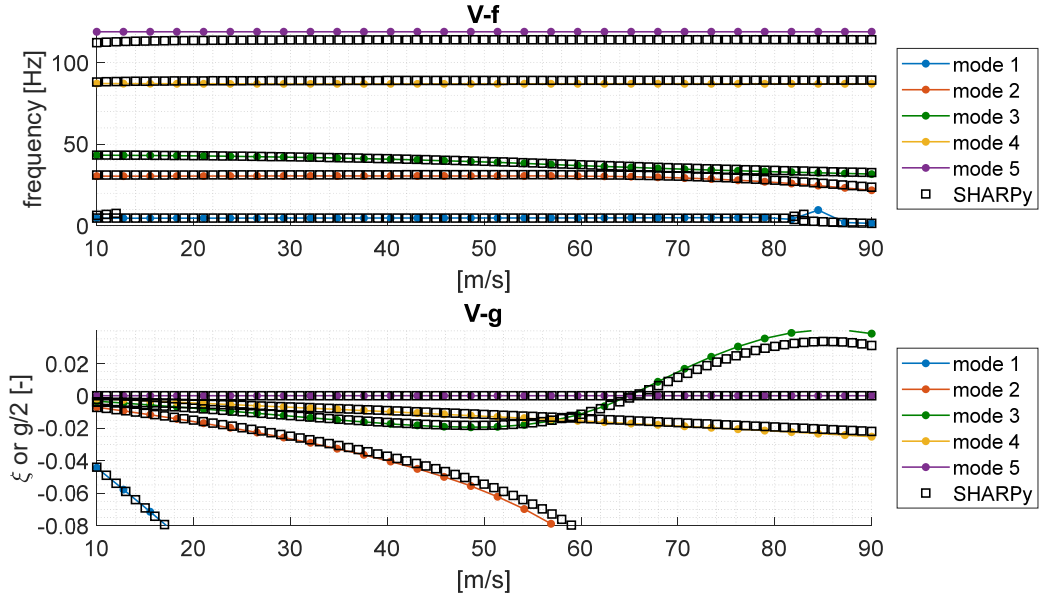

Figure 14: Linear flutter solution for NeoCASS and SHARPy, AoA=0°

The non-linear solution is then compared, e.g. for a incidence of 5° as in Figure 15, where the *V-f* and *V-ξ* plots are reported. The behavior of the flutter mechanisms is well identified: a first flutter is identified at lower speed $43\frac{m}{s} < V_{f1\,\alpha=5°} < 51\frac{m}{s}$ and a second flutter mode is identified for $V_{f2\,\alpha=5°} > 70\frac{m}{s}$. The flutter modes are the ones in Figure 16.

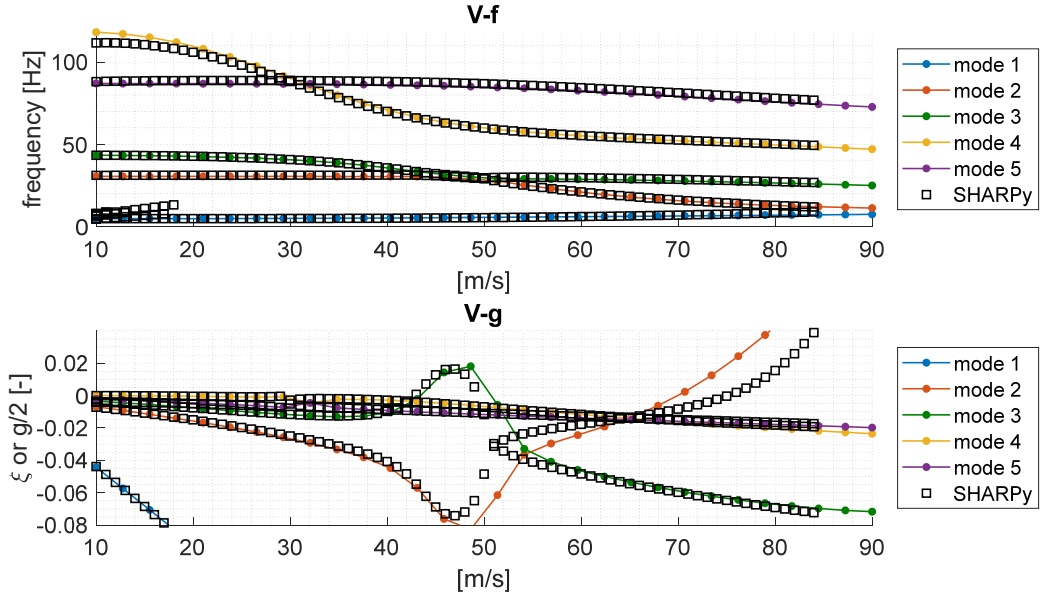*Figure 15: Non-Linear flutter solution for NeoCASS and SHARPy, AoA=5°*

| (a) | (b) |
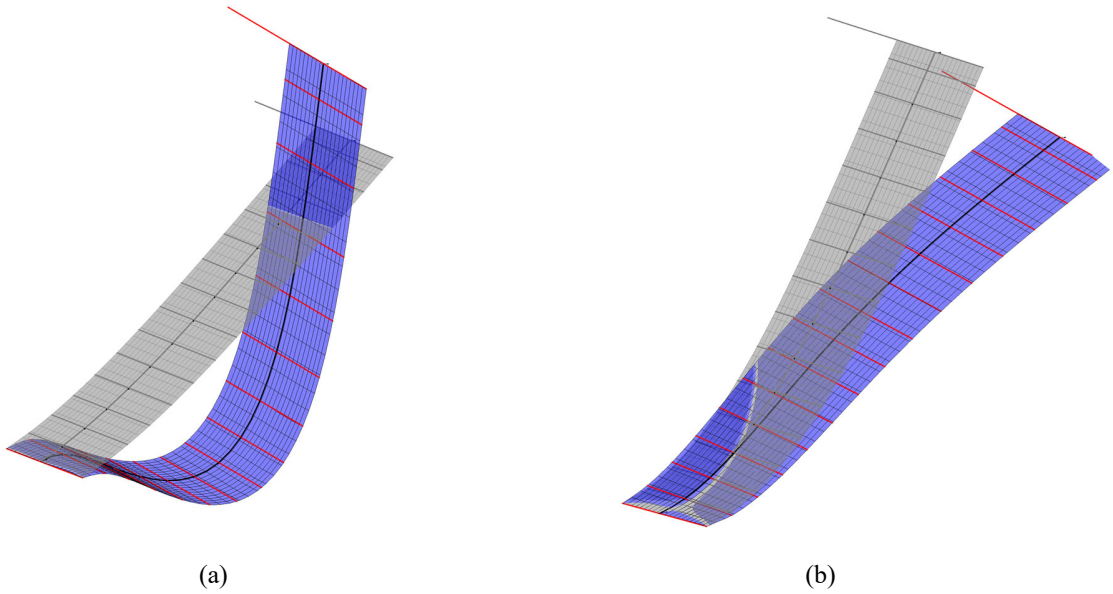
Figure 16: Flutter modes: (a) 1st flutter mode is the coupling of 2nd out of plane bending and 1st torsion; (b) 2nd flutter mode is the coupling of 1st out of plane bending and 1st torsion.

The aeroelastic behavior of the Pre-Pazy wing in the range of attitudes between 0° and 5° is resumed in Table 1 and Figure 17: Increasing the incidence it is possible to see that a flutter mechanism at 0° evolves into a hump mode that involves the 1st torsional and the 2nd out-of-plane modes. Its onset and offset velocities reduce by increasing the incidence, as listed in Table 1. A 2nd flutter mechanism arises increasing the incidence, and this time it involves the 1st torsion and the 1st out-of-plane modes. In general, the flutter is identified correctly, a little velocity shift is present

for the onset of the first flutter mode (Δ<3.5%), that is a little bigger for the flutter offset (Δ<6.3%). The presence of the 2nd flutter mode followS a similar behavior, with errors below 3.8% except for α=5°, where the error increases at 6.87%. Here must be pointed out that the aerodynamic methods (DLM vs. UVLM) and the beam models have intrinsic differences, which may lead to slightly different results.

Table 1: Flutter velocity comparison between NeoCASS and SHARPy

| α [°]	1st flutter onset			1st flutter offset			2nd flutter onset		
	NeoCASS [m/s]	SHARPy [m/s]	Δ [%]	NeoCASS [m/s]	SHARPy [m/s]	Δ [%]	NeoCASS [m/s]	SHARPy [m/s]	Δ [%]
0.00	64.95	65.00	-0.08	N/A	N/A	N/A	N/A	N/A	N/A
0.25	66.69	64.94	2.69	N/A	N/A	N/A	N/A	N/A	N/A
0.50	65.67	63.65	3.17	N/A	84.68	N/A	89.61	89.95	-0.38
1.00	62.19	60.25	3.23	80.81	76.09	6.21	86.23	85.36	1.01
2.00	55.46	54.04	2.62	68.70	65.35	5.12	80.17	79.89	0.35
3.00	50.34	49.34	2.03	60.83	58.36	4.23	75.80	76.88	-1.41
4.00	46.52	45.73	1.72	55.17	53.27	3.57	72.53	75.39	-3.80
5.00	43.48	42.87	1.43	50.73	49.31	2.87	69.99	75.16	-6.87
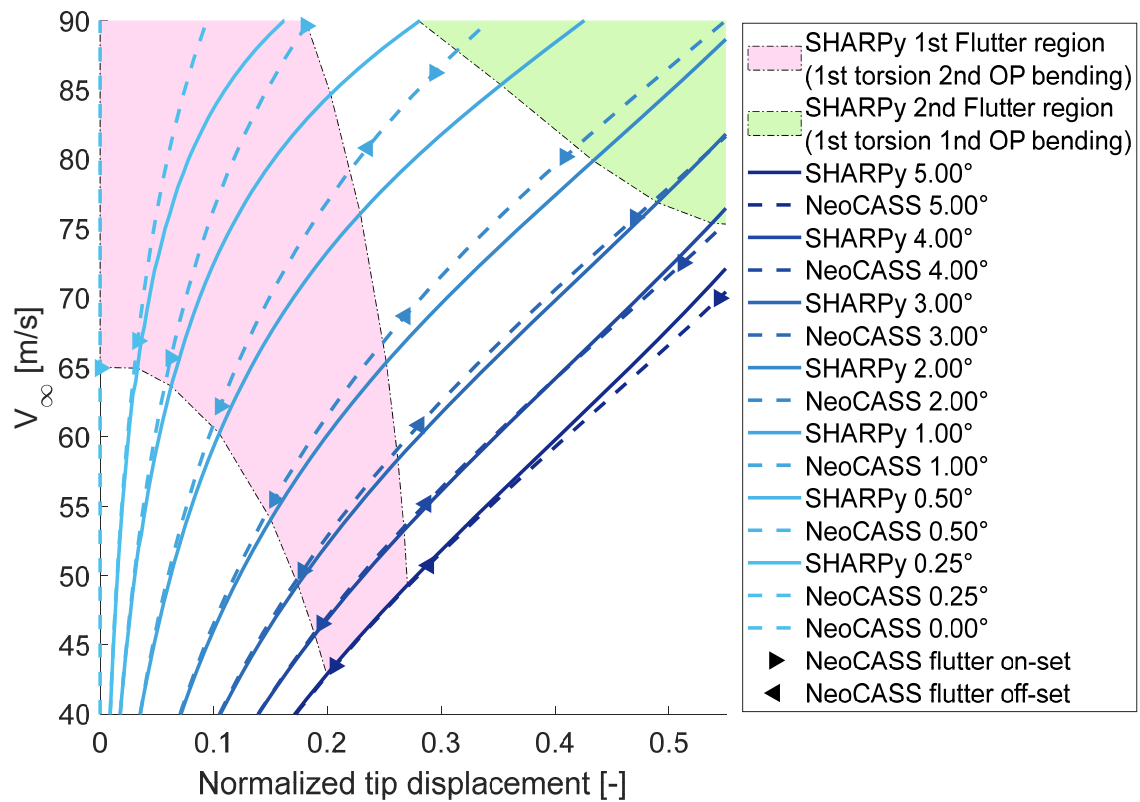
Figure 17: Flutter map for the Pre-Pazy wing

III. Conclusion

This work presented an improvement of the analysis capabilities of NeoCASS suite obtained by implementing a set of dedicated nonlinear aeroelastic solvers. They were validated with a literature known test-case, providing a good correlation with other software and experimental measures. The non-linear solvers are encompassed into the NeoCASS suite, providing a single-environment single-model tool that can be exploited by the aircraft designer since the conceptual design phases, accounting for geometrical non-linear aeroelastic effects.

The importance of non-linear aeroelastic stability analysis is remarked by the test case analyzed in this paper, where depending on the flight condition, angle of attack in this case, the flutter speed can dramatically decrease (-33% for α=5°).

Some discrepancies are still present in the presented results, the non-smooth transition of the flutter speed between the unloaded wing and the non-linear solution at very low incidence, mainly due to the re-alignment of the DLM mesh to the wind direction. This latest issue will be investigated in the future work, together with a full free-free non-linear trim solver that implements the inertial relief. Moreover, the possibility of performing aeroelastic dynamic simulations around a linearized equilibrium solution, e.g. gust, will be implemented both in frequency domain (Nastran-like) and in State-Space domain. The latest features are already available in NeoCASS and need to be patched to the non-linear solver.

IV. Acknowledgments

References

[1] Liebeck, R. H. Design of the blended wing body subsonic transport. Journal of aircraft, 2004, vol. 41, no. 1, pp. 10–25. DOI:10.2514/1.9084

[2] Lyu, Z.; Martins J. R. Aerodynamic design optimization studies of a blended-wing-body aircraft. Journal of Aircraft, 2014, vol. 51, no. 5, pp. 1604–1617. DOI:10.2514/1.c032491

[3] Su, W.; Cesnik, C. E. Nonlinear aeroelasticity of a very flexible blended-wing-body aircraft. Journal of Aircraft, 2010, vol. 47, no. 5, pp. 1539–1553. DOI: 10.2514/1.47317

[4] Johanning, A.; Scholz; D. Investigation of a Novel Turboprop-Driven Aircraft Concept Including Future Technologies. In: Bajpai, R.P.; Chandrasekhar U.: Innovative Design and Development Practices in Aerospace and Automotive Engineering, Lecture Notes in Mechanical Engineering, I-DAD, February 22 - 24, 2016. Springer. Singapore. 2017. Doi: 10.1007/978-981-10-1771-1_62

[5] Jansen, R.; Bowman, C.; Jankovsky, A.; Dyson, R.; Felder, J. Overview of NASA electrified aircraft propulsion (EAP) research for large subsonic transports. In 53rd AIAA/SAE/ASEE Joint Propulsion Conference, p. 4701, 2017. DOI: 10.2514/6.2017-4701

[6] Gur, O.; Bhatia, M.; Schetz, J. A.; Mason, W. H.; Kapania, R. K.; Mavris, D. N. Design optimization of a truss-braced-wing transonic transport aircraft. Journal of aircraft, 2010, vol 47(6) ,pp. 1907-1917. DOI: 10.2514/1.47546

[7] Bradley, M. K.; Droney, C. K.; Allen, T. J. Subsonic ultra-green aircraft research (No. NF1676L-19776). Available online: https://ntrs.nasa.gov/api/citations/20120009038/downloads/20120009038.pdf (Accessed on 10/11/2022)

[8] TU Delft, "Flying V." Available online: https://www.tudelft.nl/en/ae/flying-v/. (Accessed on 25/10/2022)

[9] Frediani, A., Cipolla, V., Rizzo, E. The PrandtlPlane Configuration: Overview on Possible Applications to Civil Aviation. In: Variational Analysis and Aerospace Engineering: Mathematical Challenges for Aerospace Design. Springer Optimization and Its Applications, vol 66. Springer, Boston, MA, USA. DOI:10.1007/978-1-4614-2435-2_8

[10] Cavallaro, R; Bombardieri, R.; Demasi, L.; Iannelli, A. Prandtlplane joined wing: Body freedom flutter, limit cycle oscillation and freeplay studies. Journal of Fluids and Structures, 2015, vol. 59, pp. 57–84. DOI:10.1016/j.jfluidstructs.2015.08.016

[11] Kenway, G.; Kennedy, G.; Martins, J. R. Aerostructural optimization of the Common Research Model configuration. In 15th AIAA/ISSMO multidisciplinary analysis and optimization conference 2014 (p. 3274). DOI:10.2514/6.2014-3274

[12] Brooks, T. R.; Kenway, G. K.; Martins, J. R. Undeflected common research model (uCRM): an aerostructural model for the study of high aspect ratio transport aircraft wings. In 35th AIAA Applied Aerodynamics Conference 2017 (p. 4456). DOI:10.2514/6.2017-4456

[13] Ricci, S.; Paletta, N.; Defoort, S.; Benard, E.; Cooper, J. E.; Barabinot, P. U-HARWARD: a CS2 EU funded project aiming at the Design of Ultra High Aspect Ratio Wings Aircraft. In AIAA Scitech 2022 Forum (p. 0168). DOI:10.2514/6.2022-0168

[14] Ricci, S.; Marchetti, L.; Toffol, F.; Beretta, J.; Paletta, N. Aeroelastic Optimization of High Aspect Ratio Wings for Environmentally Friendly Aircraft. In AIAA Scitech 2022 Forum (p. 0166). DOI:10.2514/6.2022-0166

[15] Roeseler, W. G.; Sarh, B.; Kismarton, M. U.; Quinlivan, J.; Sutter, J.; Roberts, D. (2007, July). Composite structures: the first 100 years. In 16th International Conference on Composite Materials (pp. 1-41). Japan Society for Composite Materials Kyoto, Japan. DOI:10.1201/9780367812720-3

[16] Cesnik, C. E., Palacios, R., & Reichenbach, E. Y. (2014). Reexamined structural design procedures for very flexible aircraft. Journal of Aircraft, 51(5), 1580-1591.

[17] Riso, C., Di Vincenzo, F. G., Ritter, M., Cesnik, C. E., & Mastroddi, F. (2018). Nonlinear aeroelastic trim of very flexible aircraft described by detailed models. Journal of Aircraft, 55(6), 2338-2346.

[18] Ritter, M., Cesnik, C. E., & Krüger, W. R. (2015). An enhanced modal approach for large deformation modeling of wing-like structures. In 56th AIAA/ASCE/AHS/ASC Structures, Structural Dynamics, and Materials Conference (p. 0176).

[19] del Carre, A., Muñoz-Simón, A., Goizueta, N., & Palacios, R. (2019). SHARPy: A dynamic aeroelastic simulation toolbox for very flexible aircraft and wind turbines. Journal of Open Source Software, 4(44), 1885.

[20] Hilger J, Ritter MR. Nonlinear Aeroelastic Simulations and Stability Analysis of the Pazy Wing Aeroelastic Benchmark. Aerospace. 2021; 8(10):308. https://doi.org/10.3390/aerospace8100308

[21] Ritter, M., Hilger, J., & Zimmer, M. (2021). Static and dynamic simulations of the Pazy wing aeroelastic benchmark by nonlinear potential aerodynamics and detailed FE model. In AIAA Scitech 2021 Forum (p. 1713).

[22] Drachinsky, A., & Raveh, D. E. (2020). Modal rotations: A modal-based method for large structural deformations of slender bodies. AIAA Journal, 58(7), 3159-3173.

[23] Drachinsky, A., & Raveh, D. E. (2022). Nonlinear Aeroelastic Analysis of Highly Flexible Wings Using the Modal Rotation Method. AIAA Journal, 60(5), 3122-3134.

[24] Werter, N. P. M., & De Breuker, R. (2016). A novel dynamic aeroelastic framework for aeroelastic tailoring and structural optimisation. Composite Structures, 158, 369-386.

[25] Piperni, P., DeBlois, A., & Henderson, R. (2013). Development of a multilevel multidisciplinary-optimization capability for an industrial environment. AIAA journal, 51(10), 2335-2352.

[26] Autry, Brenden A., and Danilo Victorazzo. "Automated top level aircraft structural sizing tool (Atlass): A framework for preliminary aircraft design and optimization." AIAA Scitech 2019 Forum. 2019.

[27] Elham, A. (2013). Weight indexing for multidisciplinary design optimization of lifting surfaces.

[28] L. Cavagna, S. Ricci, and L. Travaglini, "Neocass: an integrated tool for structural sizing, aeroelastic analysis and mdo at conceptual design level," Progress in Aerospace Sciences, vol. 47, no. 8, pp. 621–635, 2011.

[29] L. Cavagna, S. Ricci, and L. Travaglini, "Structural sizing and aeroelastic optimization in aircraft conceptual design using neocass suite," in 13th AIAA/ISSMO Multidisciplinary Analysis Optimization Conference, p. 9076, 2010.

[30] L. Cavagna, S. Ricci, and L. Riccobene, "A fast tool for structural sizing, aeroelastic analysis and optimization in aircraft conceptual design," in 50th AIAA/ASME/ASCE/AHS/ASC Structures, Structural Dynamics, and Materials Conference 17th AIAA/ASME/AHS Adaptive Structures Conference 11th AIAA No, p. 2571, 2009.

[31] L. Cavagna, S. Ricci, and L. Riccobene, "Structural sizing, aeroelastic analysis, and optimization in aircraft conceptual design," Journal of Aircraft, vol. 48, no. 6, pp. 1840–1855, 2011.

[32] Fonte, F.; Ricci, S. Recent developments of NeoCass the open-source suite for structural sizing and aeroelastic analysis. In 18th International Forum on Aeroelasticity and Structural Dynamics (IFASD 2019), 2019.

[33] Toffol, F.; Ricci, S. Wingbox Meta-Model and Aero-Servo-Elastic Optimization With NEOPT. In International Conference on Multidisciplinary Design Optimization of Aerospace Systems (AeroBest 2021) (pp. 1-15). IDMEC, 2021.

[34] Toffol, F., Ricci, S.,NeOPT: an Optimization Suite for the Aeroelastic Preliminary Design. In 18th International Forum on Aeroelasticity and Structural Dynamics (IFASD 2019).

[35] Toffol, F. Aero-servo-elastic optimization in conceptual and preliminary design. PhD Thesis, Politecnico di Milano, Milano, 2021

[36] Toffol, F.; Ricci, S. A Meta-Model for Composite Wingbox Sizing in Aircraft Conceptual Design. *Composite Structure*, 2022 (submitted).

[37] Ghiringhelli, Gian Luca, Pierangelo Masarati, and Paolo Mantegazza. "Multibody implementation of finite volume C beams." AIAA journal 38.1 (2000): 131-138.

[38] Avin, O., Raveh, D. E., Drachinsky, A., Ben-Shmuel, Y., & Tur, M. (2021). An experimental benchmark of a very flexiblewing. In AIAA Scitech 2021 Forum (p. 1709).

[39] Aeroelastic Prediction Workshop #3 (AePW3) Large Deflection Working Group (LDWG) https://nescacademy.nasa.gov/workshops/AePW3/public/wg/largedeflection

[40] Goizueta, N., Wynn, A., Palacios, R., Drachinsky, A., & Raveh, D. E. (2022). Flutter predictions for very flexible wing wind tunnel test. Journal of Aircraft, 1-16.

[41] Riso, C., & Cesnik, C. E. (2021). Correlations Between UM/NAST Nonlinear Aeroelastic Simulations and the Pre-Pazy Wing Experiment. In AIAA Scitech 2021 Forum (p. 1712).

[42] Beckert, A., & Wendland, H. (2001). Multivariate interpolation for fluid-structure-interaction problems using radial basis functions. Aerospace Science and Technology, 5(2), 125-134.

[43] Mantegazza, P. (2011). Tutorial on attached-mean axes and their use in the calculation of deformable static and damped-undamped vibration modes of a free-free structure. Journal of Aeroelasticity and Structural Dynamics, 2(1).

[44] Albano, E., & Rodden, W. P. (1969). A doublet-lattice method for calculating lift distributions on oscillating surfaces in subsonic flows. AIAA journal, 7(2), 279-285.

[45] Cardani, C.; Mantegazza, P. "Continuation and Direct Solution of the Flutter Equation". Computer and Structures, 1978, Vol. 8, pp.185-192